Development of Wide-Area Mineral Identification System Using Multispectral Camera Mounted on Drone for Beach Placer Deposits

Hiromasa Nozaki[1], Natsuo Okada[1], Brian Bino Sinaice[2], Yoko Otomo[3], Youhei Kawamura[3]

[1] Graduate School of Engineering, Hokkaido University, Kita13, Nishi8, Kita-ku, Sapporo, Hokkaido 060-8628, Japan
[2] Graduate school of International Resource Sciences, Akita University, 1-1 Tegata-gakuenmachi, Akita, Akita Prefecture 010-8502, Japan
[3] Faculty of Engineering, Hokkaido University, Kita13, Nishi8, Kita-ku, Sapporo, Hokkaido 060-8628, Japan

Abstract. Iron sand, a valuable mineral found in placer deposits, is difficult to identify and extract due to the constantly changing nature of beach placer deposits. Traditional visible light cameras mounted on drones are insufficient for identifying specific rocks and minerals. However, hyperspectral cameras provide more comprehensive assessments but can be bulky and time-consuming for data processing. A recent approach involving specialized multispectral bands has emerged as a solution to the disadvantages of hyperspectral imaging. This study proposes using a 6-band DJI P4 multispectral drone and Convolutional Neural Networks (CNN) to automatically identify the composition of mineral sand from the placer deposit located in Kunisaki peninsula, Japan. The combination of multispectral imaging and deep learning techniques has the potential to optimize several aspects of the mining chain, making it an attractive area of research. This study aims to evaluate an efficient approach for the automatic identification of mineral sand composition, using a commercial drone equipped with a multispectral camera, driving towards a more efficient and accurate mineral exploration and extraction processes for the mining industry.

Keywords: Smart mining, Surface mining, Multispectral, Deep learning, Drone, Placer deposit, Iron sand, Mineral sand.

1 Introduction

1.1 Benefits of employing AI methods in Mineral Identification

In recent years, the use of unmanned automated vehicles (UAVs), such as drones, for remote sensing in mines has become increasingly important due to the advantages such as the ability to cover a wide range of areas, high safety, and the ability to obtain high spatial resolution[1,2]. However, when it comes to identifying certain rocks or minerals in a mine site, a visible light camera mounted on a drone is often insufficient. This is

© The Author(s) 2023
A. Lkhamsuren et al. (eds.), *Proceedings of the Second International Conference on Resources and Technology (RESAT 2023)*, Advances in Engineering Research 226,
https://doi.org/10.2991/978-94-6463-318-4_17

because such cameras may be limited to capturing only the visible light spectrum that they do not collect the intrinsic characteristics of rocks and minerals beyond this range [3,4]. As a result, more advanced techniques and technologies are needed to address this limitation and enable more comprehensive assessments of mine sites. To address the limitations of using visible light cameras mounted on drones for mine site assessments, the use of hyperspectral cameras for remote sensing has become increasingly prevalent. Hyperspectral imaging is already being applied in a variety of fields, including industry, agriculture, bioscience, and remote sensing. However, the equipment required for hyperspectral imaging can often be bulky and data processing can be time-consuming [5,6,7], which presents significant challenges. Recent research has shown that using a few specialized multispectral imaging bands can provide similar high subject resolving power for classifying rocks and minerals [8]. This approach involves reducing the dimensionality of hyperspectral imaging by using specialized multispectral bands, which eliminates the disadvantages associated with hyperspectral imaging [9]. Previous studies [10,11,12], have also utilized a method that involves the remote collection of vegetation data via a MS camera mounted on a UAV drone, in order to identify specific vegetation species. Building upon this methodology, a novel approach has been developed to enable the identification of rocks and minerals in large-scale areas with detailed field assessments. This proposed method combines MS mounted UAV drone technology with Convolutional Neural Networks (CNN) to automatically identify the composition of mineral sand. The combination of MS imaging and deep learning techniques has the potential to optimize several aspects of the mining chain, making it an attractive area of research. For this reason, this paper introduced 'DJI P4 multispectral drone' based on the currently available industry produced spectral imaging devices used in agricultural applications and environmental monitoring to identify the appropriate rock classifying multispectral bands. The main objective of this study is to evaluate an efficient approach for the automatic identification of mineral sand composition, using a commercial drone equipped with a MS camera.

Mineral sand is a term used to describe a mineral resource consisting mainly of titanium oxide minerals, such as ilmenite and rutile, with titanium (Ti) as the primary component, and zirconium oxide minerals, such as zircon, with zirconium (Zr) as the primary component. These minerals, along with rare earths and lithium, which have been attracting attention in recent years, are used in various products essential to our daily lives. These minerals can be found in placer deposits in countries such as Australia, South Africa, and Sierra Leone, and iron sand is also an important constituent found in placer deposits. Since ancient times, iron sand has been collected in many parts of Japan [13], including the coast of the Kunisaki Peninsula. It is estimated that there are thousands to tens of thousands of tons of iron sand buried in the Kunisaki Peninsula placer deposits and the black area, which is believed to be where iron sand is densely concentrated, is visible through aerial photography using a drone. However the mine is no longer in operation and has been abandoned. Unlike other types of mineral deposits, beach placer deposits are constantly changing due to the water flow in oceans, making it difficult to manage production volume and quality.

This paper is focusing on verifying the effectiveness of this approach in identifying mineral compositions in placer deposits, while also discussing the preprocessing and

analytical techniques required for deep learning using data obtained from the MS camera. Positive results from this research, utilizing a novel method that combines MS camera mounted drone and CNN, would aid in ascertaining the feasibility of field applications. Hence, demonstrating the effectiveness and potential of this approach, ultimately leading to more efficient and accurate mineral exploration and extraction processes in the mining industry.

1.2 Study Area

In this study, the experiment was conducted in the 9th Kumano mining area, which exhibited the highest concentration of iron sand among several mining sites (Fig..1) Iron

Fig. 1. Map showing the 9th Kumano magnetite iron sand placer deposits located on Kunisaki peninsula, Oita prefecture, Japan. Red square represents the study area within which the UAV drone was flown. Map acquired from: Google Earth (2023).

sand deposits are mainly composed of sand dune sediments, and the amount of iron sand deposited varies significantly depending on the time period.

The iron sand deposits on the coast of the Kunisaki Peninsula are placers, which can be divided into two types: beach iron sand deposits that are washed up on the current

coastline by the formation process and coastal dune iron sand deposits that accumulate in sand dunes. The study area is beach iron sand deposit located on the eastern coast of the Kunisaki Peninsula, in the eastern part of Oita Prefecture, Japan (Fig. 1). The Mt. Futagosan volcano group, which occupies the main part of the Kunisaki Peninsula, is composed of a central lava dome group and volcanic debris surrounding it. The volcanic debris forms a dissected alluvial fan at the foot of the mountain and is mainly composed of pyroclastic flow deposits in the central part of the volcano and lahars in the peripheral part. The iron sand include plagioclase, orthoclase, quartz, pyroxene, clinopyroxene, hornblende, biotite, calcite, garnet, and monazite. The ore minerals are mainly composed of magnetite, ilmenite, and hematite[14].

2 Proposed system

This study evaluate an efficient approach for the automatic identification of mineral sand composition, using a commercial drone equipped with a MS camera and to verify the effectiveness of this approach in identifying mineral compositions in placer deposits. On the other hand, this verification is essential for developing a system using a MS technique for drone-based exploration of large-scale spaces, such as mineral sand deposits, and identifying target minerals and other valuable minerals using aerial exploration by drones. Fig. 2 shows an overview of the useful mineral broad mapping system by drone. The system involves capturing images of the mineral deposits using the MS camera mounted on the drone, and mapping the target minerals and other useful minerals in a way that can be easily visualized through color coding.

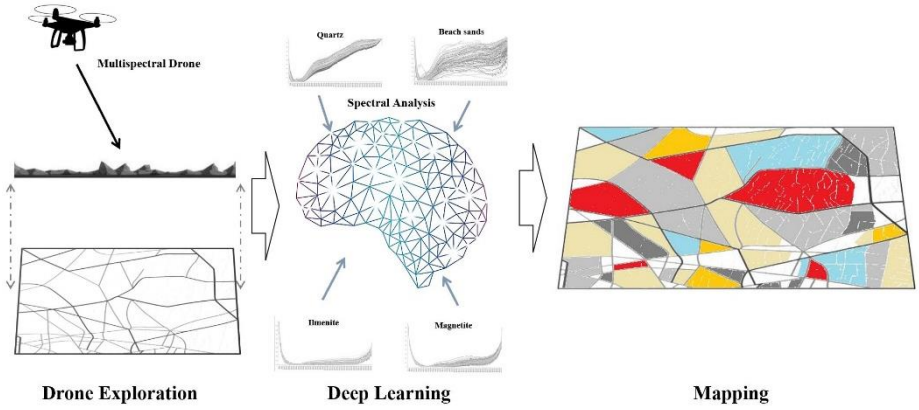

Fig. 2. Overview of the mineral mapping system.

MS cameras are used for aerial photography by drones. The data captured by the MS camera is analyzed through deep learning, CNN, to identify various minerals. Prior to training the AI algorithms, pre-processing of the data is conducted. Data pre-processing is crucial as it helps to clean the data and make it more interpretable for the algorithms. This brain is then generated through CNN to identify the reference/target by learning the spectral data of the mineral species.

This process, referred to as image segmentation, involves the labeling of each pixel in a captured image [5]. The pixels within the mask that represent the ground truth are labeled as target, while the unmasked pixels from the image are labeled as noise. By using labeled datasets, algorithms can leverage both the global and local structures of the data [15]. For each image, the CSV file contains labeled ground truth pixels (magnetite, ilmenite and so on) as well as noise pixels (beach sands). Using this data as input, the algorithms are subsequently trained, and the outputs pertaining to the classification capabilities of the models in deducing mineral compositions are presented.

3 Methodology

3.1 Multispectral Imaging

Hyperspectral imaging has been regarded as one of the most effective methods to identify rocks and minerals based on their spectral characteristics [16]. However, previous research [17] has demonstrated that similar rock identification problems can be solved with high-accuracy outputs using multispectral imaging. Inspired by the promising multispectral capabilities, this paper employs a UAV drone equipped with a multispectral camera (Fig. 3). The spectral sensor specifications are as follows: Blue: 450 nm ± 16 nm, Green: 560 nm ± 16 nm, Red: 650 nm ± 16 nm, Red Edge (RE): 730 nm ± 16 nm, Near Infrared (NIR): 840 nm ± 26 nm, which are all captured as TIFF image files. The drone has a 62.7° field of view, a net weight of 468 g, and an RGB camera that facilitates the extraction of spectral information in the visible light spectral range of 400-700 nm as a JPG image. This makes the system effective in a wide range of electromagnetic spectra within the visible-near-infrared range (VNIR), with a total of 6 multispectral bands.

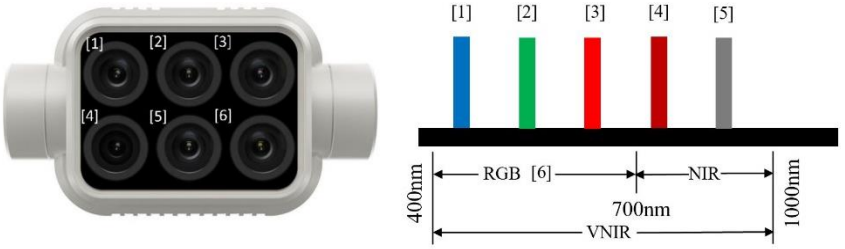

Fig. 3. The 6 bands multispectral sensor with a 62.7° field of view; [1] Blue: 450 nm ± 16 nm, [2] Green: 560 nm ± 16 nm, [3] Red: 650 nm ± 16 nm, [4] Red Edge: 730 nm ± 16 nm, [5] Near Infrared: 840 nm ± 26 nm and [6] RGB camera: 400-1000 nm represent the multispectral sensor capabilities.

3.2 Remote Sensing

Drone technology has evolved over the years, with recent developments catering to specialized industrial applications. One of the advantages of UAV drones is the protection of human life as sites can be assessed from a remote area [18,19]. In addition, camera mounted drones aid in real time assessments of sites via visual feed. This feed can be in the form of real, false or manipulated colors which are preprogrammed to represent a certain phenomenon understood by the operator [20]. One of the image analysis techniques used in remote sensing is the multispectral method. This method takes advantage of the fact that every substance on earth reflects electromagnetic waves in a unique way, which is known as its spectral characteristic. By analyzing the spectral characteristics of a substance, its characteristics and the composition can be identified. While the human eye can only observe the visible range of the electromagnetic spectrum, multispectral cameras can continuously observe spectral characteristics in the visible, near-infrared, and shortwave infrared range (400-2500 nm) with a resolution of less than 10 nm. However, the trade-off of increasing the number of wavelengths with hyperspectral (HS) sensors is that the observation area becomes narrower and the number of sensors used in operations is limited. Consequently, the amount of observation data archived with HS sensors is limited compared to MS sensors, and there are many unobserved areas.

As a result, other industries and academic organizations have been motivated to improve and utilize aerial investigation technologies due to the significant benefits of high-resolution spectral imaging compared to traditional color imaging techniques, as such, multispectral sensors are seeing application in mineral identification procedures through remote sensing, as observed in several studies [21,22].

3.3 Deep Learning Network

Deep learning techniques, particularly those using convolutional neural networks (CNNs), have become state-of-the-art in many applications [23], including remote sensing and geotechnical engineering [24]. This is due to their ability to learn feature representations and classify patterns in data, making them superior to traditional handcrafted techniques. The use of CNNs has been proposed for rock classification based on hyperspectral signatures. Although deep learning models require large amounts of data and refinement, they have shown significant success in various vision tasks [25,26].

A typical CNNs has three main layers: an input layer where raw data is located, a hidden layer housing convolution layers that detect and locate localized features, and an output layer that presents network performance results. The hidden layer also includes a maximum pooling layer, which compresses localized feature extractions and reduces computational costs. A typical architecture of a VGG 16 CNN model is shown in Fig. 4. This VGG16 architecture consists of 13 convolutional layers and 3 fully connected layers. In the figure, the input image size is 224×224, and it becomes 7×7 after passing through the convolutional layers.

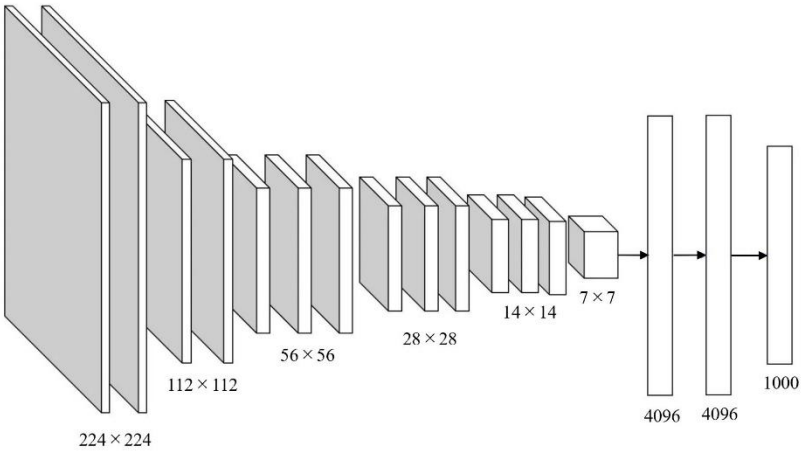

Fig. 4. An example of a VGG16 architecture consisting of 13 convolutional layers and 3 fully connected layers. In this diagram, the input image size is 224×224, and it becomes 7×7 after passing through the convolutional layers.

4 Experiments

4.1 Indoor Experiments, Capturing Rock's Multispectral Signatures

First, XRD analysis was conducted on the beach sand contained within the black sand layer collected from the field. The results are shown in Fig. 5, revealing the presence of quartz, magnetite, ilmenite, and pyroxene. In addition to the sample collected from

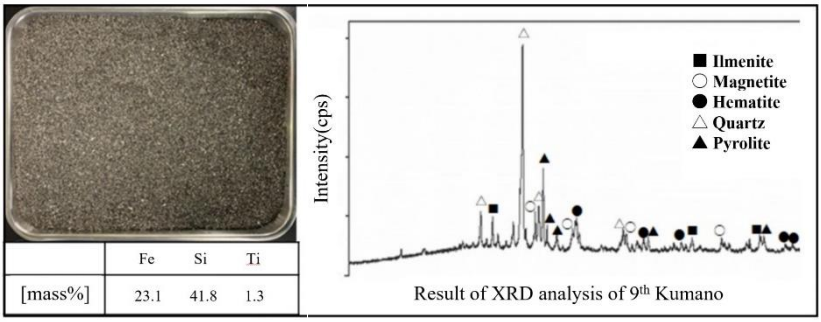

Fig. 5. Result of XRD analysis of the beach sand collected from 9th Kumano.

the field, rock specimens containing quartz, albite, Anorthite, magnetite, ilmenite, Augite Hornblende, and Hematite were prepared, as observed through microscopic analysis (Fig. 6).

Fig. 6. Rock specimens of Hematite (a), Augite(b), Anorthite(c), Magnetite(d), Albite(e), Hornblende(f), Ilmenite(g), and quartz(h).

Next, the prepared samples were photographed using an MS camera in a darkroom. The target minerals were illuminated from three directions (left, right, and behind the camera) using halogen lights, which provided a uniform illumination in the wavelength range of 400–1,000 nm, the range that the camera can capture. The main components of the spectral data extraction setup are shown in Fig. 7. Although the filament part of the halogen light is heated to a very high temperature over time and the wavelength peak of the halogen shifts to a higher value, no significant impact on the acquired

spectral data was observed during the several hours of use, which was ignored in this study. The lighting position was adjusted to prevent shadows from occurring on the minerals. Although the illumination intensity was set to a constant level in this study, the exposure time was automatically adjusted by the camera, and therefore, precise illumination settings were not necessary. The photographs were taken from 40 cm above the target.

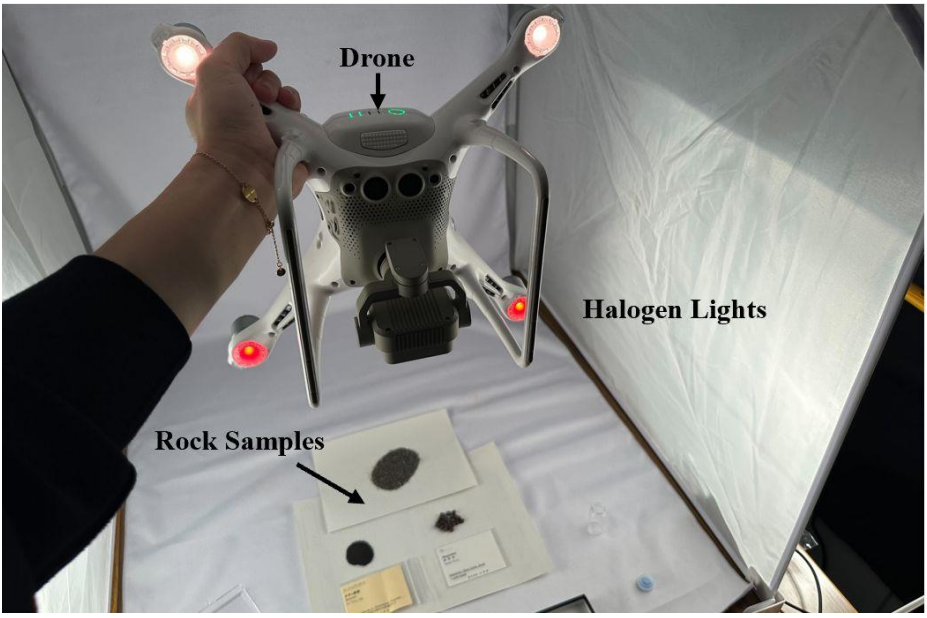

Fig. 7. Indoor experimental set-up using P4 multispectral. The drone captures MS data and sends it to the computer, data is then used for various types of analysis.

4.2 Outdoor experiments, Drone Shooting

P4 Multispectral drone equipped with an MS camera was used to capture images of the coastline along the Kunisaki Peninsula during the daytime. The focus of the capture was on the black areas where the concentration of iron sand was believed to be high. The images were taken at a height of 50m. Each capture produced five TIF files corresponding to each spectral sensor, as well as one RGB JPG file (Fig. 8).

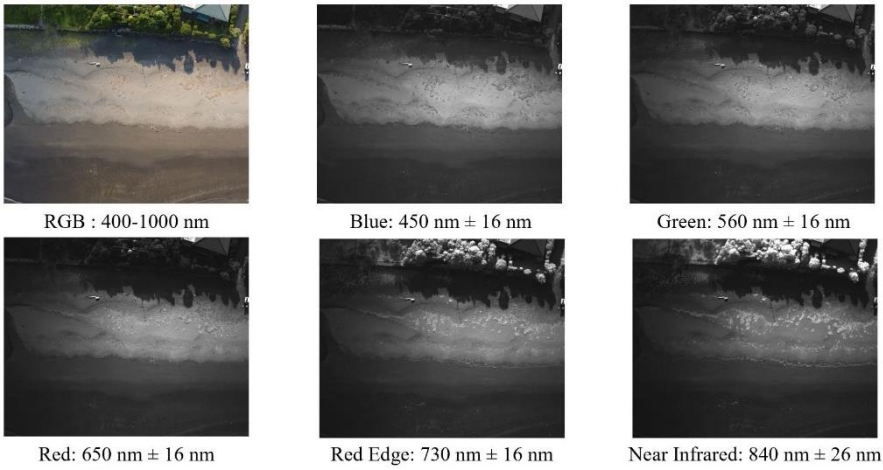

Fig. 8. Images captured by the 6 multispectral band sensors.

5 Experimental and Analytical Results

5.1 Data Pre-processing

To ensure that all sensors are aimed at the same image scene, parallax error correction is always necessary due to the small distance between the 5 spectral sensors of the drone. In this experiment, feature point matching, the process of associating characteristic features extracted from different images and correcting the parallax error, was performed on five TIF images taken from different positions. Using one TIF image as a reference point, the positions of the remaining four images were aligned (Fig. 9). Each band is displayed with a color code, and the parallax error between the images has been successfully corrected. Subsequently, these five TIF images were stacked to create a data cube. The data cube has 1600 x 1300 pixels in the x and y directions and contains information on five bands: RED, BLUE, GREEN, RE, and NIR in the z direction. The parts of the data cube that show minerals were selected, and the wavelength was extracted for each pixel. In Fig. 10, 10 pixels are selected, and their respective locations, corresponding wavelengths, and intensities are displayed below. These data were all extracted as CSV files. This process extracted 10000 training data points for each mineral.

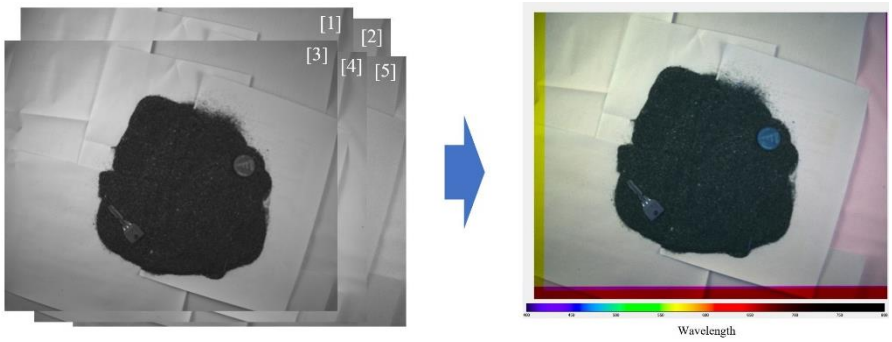

Fig. 9. Feature matching of the MS images captured.

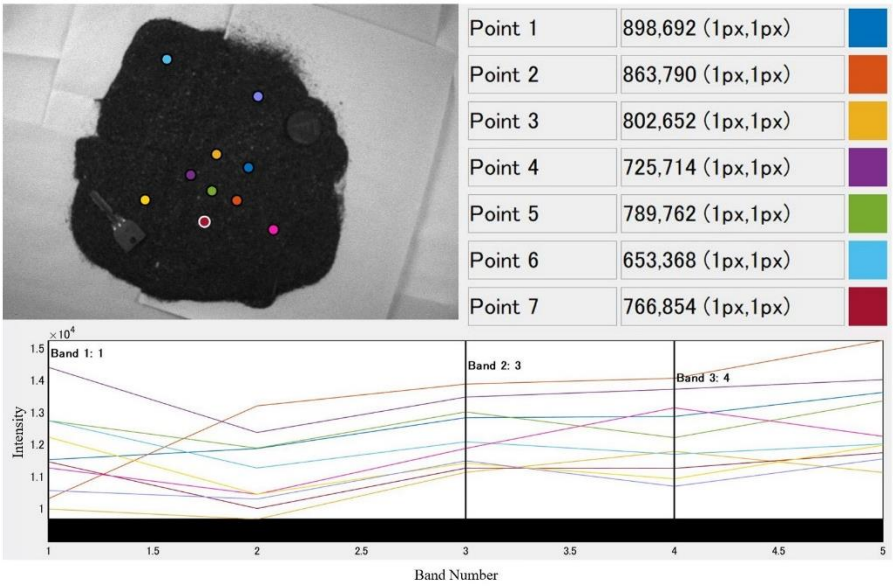

Fig. 10. Pixels selection and their corresponding wavelengths and intensities.

5.2 Classification via Deep Learning CNN

We utilized a 2D CNN with a total of 21 layers (Fig. 11). Convolutional layers are used to extract features from input image data by performing convolutional operations using filters and by stacking convolutional and pooling layers, the network can identify stronger features in images, allowing it to accurately classify multiple complex images. For instance, the first line of code "convolution2dLayer([1 3],64,'Stride',1,'Padding',[0 1])" defines a 2D convolutional layer with a kernel size of [1 3], 64 filters, a stride of 1, and padding of [0 1] in a CNN.

The training data for the input comprised a total of 60,000 data sets, with 10,000 data for each of the six mineral types The three white and colorless minerals, Quartz, Albite,

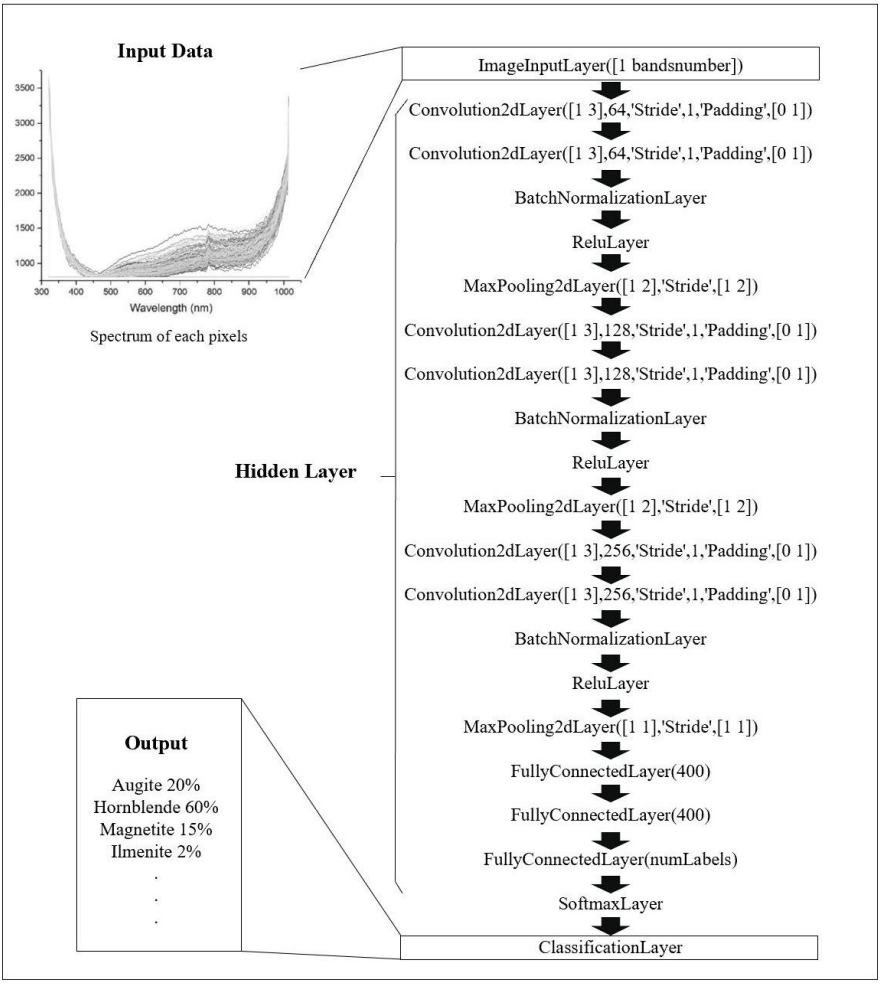

Fig. 11. The structure of the 2D CNN with input, hidden and output layers.

and Anorthite, were combined and referred to as "white sands" and the other colored minerals, including magnetite, ilmenite, augite hornblende, and hematite, were trained with their original names. Based on the five wavelengths of each mineral obtained from the MS camera, a model (brain) for identifying the minerals, referred to as MSdatanet, was trained. Fig. 12. Illustrates the training progress and the confusion matrix of the MSdatanet model. A confusion matrix is a table that summarizes the classification results by comparing the predicted and true labels of a machine learning model. For example, 90.2% of the initial input magnetite datasets (for 5-bands) were correctly classified as magnetite. On the other hand, the remaining 9.8% was incorrectly classified as augite (1.5%), hematite (0.5%), hornblende (0.6%), ilmenite (0.1%), and white sands (0%). As a result, the brain that can classify six types of minerals with a validation accuracy of 79.65% was obtained.

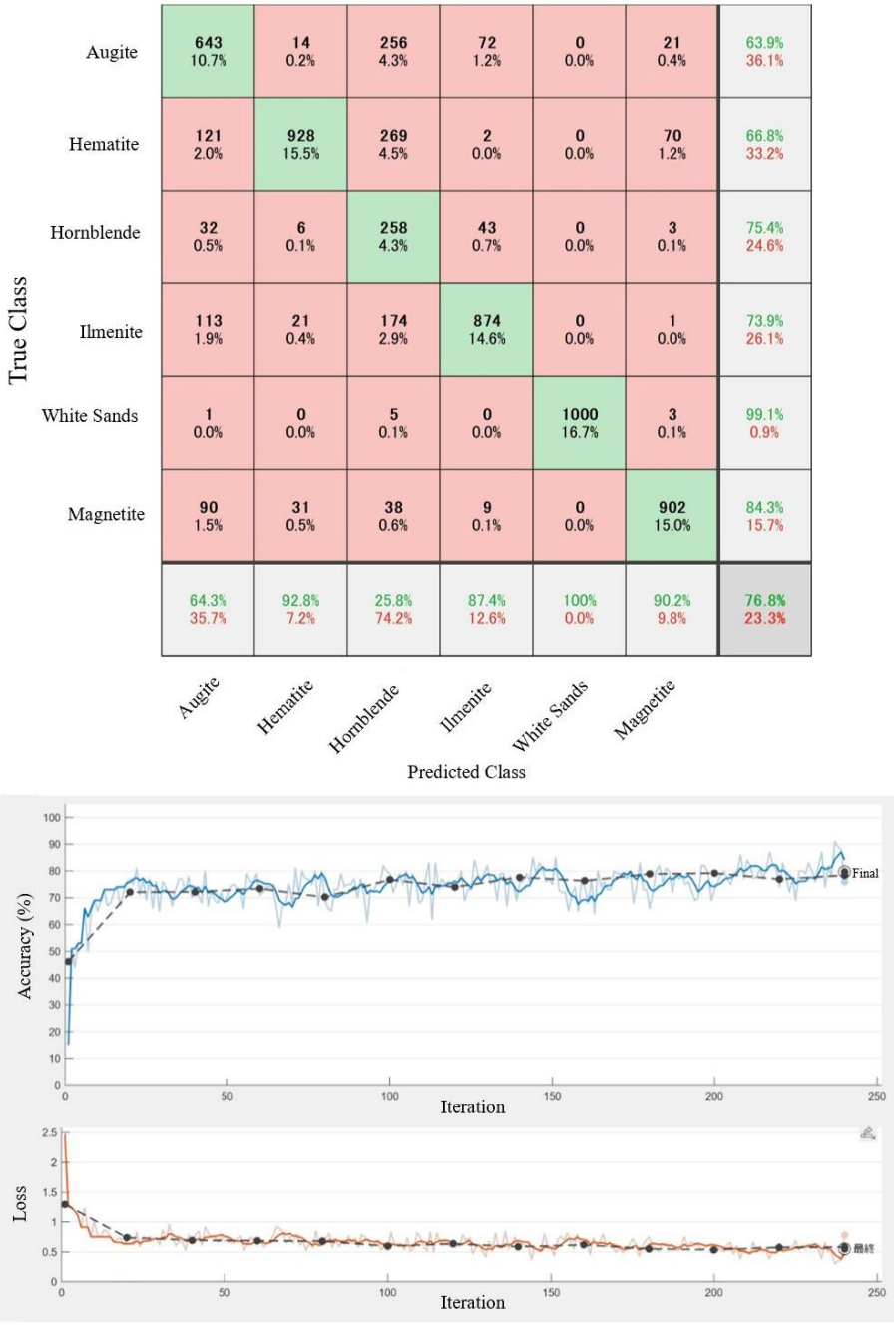

Fig. 12. Training progress and the confusion matrix of the trained MSdatanet model.

Next, the ability of MSdatanet to identify five types of colored minerals in an image was verified using a color map display. In this experiment, since the minerals being captured were already known, it was expected to reveal how accurate the MSdatanet model can identify the minerals. Each pixel is colored to correspond to the identified mineral(Fig. 13). From this figure, it is evident that MSdatanet model successfully distinguishes between the five minerals and the background. However, the identification of the five minerals is not very accurate, with most being identified as hornblende or augite. On the other hand, the part of magnetite is assigned the correct color of orange. This matches the learning results mentioned earlier, as the identification of hornblende and augite was difficult while magnetite was identified with almost 90% accuracy. Therefore, while this model has difficulty in identifying colored minerals, it is excellent as a model for identifying magnetite.

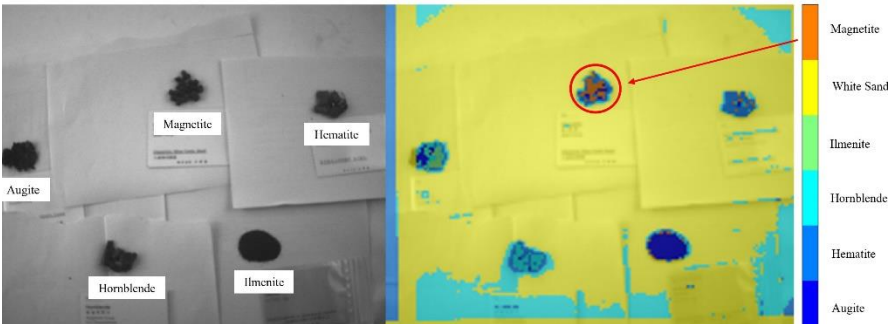

Fig. 13. The result of identifying five minerals using MSdatanet.

Finally, we used the MSdatanet model to identify minerals in sand samples collected from Kunisaki Peninsula, the 9th Kumano area. In contrast to the previous experiment, it was unknown which part of the beach sand in the sample corresponded to each mineral. In the upper right and lower left, a coin and a key were placed for feature matching, and the sand collected from the site covers the entire image. Similarly, to the previous experiment, each pixel is colored according to the mineral identified (Fig. 14). The coin, key, and background are clearly distinguished from the sand, and each mineral identified in the sand is assigned a specific color. Most of the lower left part of the figure is colored orange, indicating that magnetite is distributed in large quantities, while other parts are identified as containing augite and hornblende. Based on the XRD analysis results in section 4.1, the mass ratio of Fe is about 25%, so this result seems reasonable. Therefore, the MSdatanet model is capable of identifying magnetite among the minerals captured by P4 multi and identifying magnetite from the 9th Kumano sand sample.

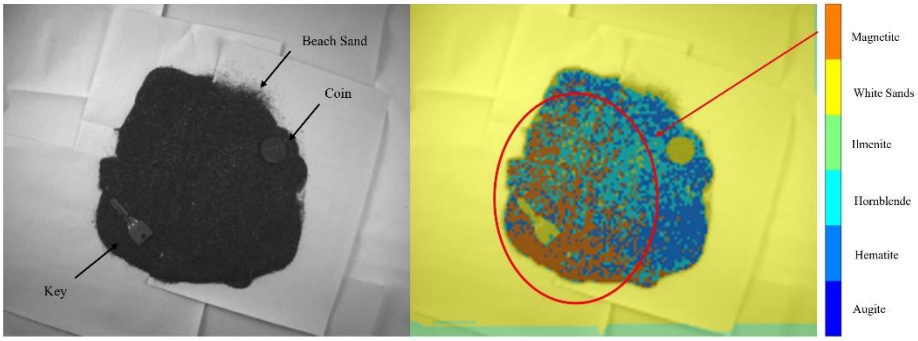

Fig. 14. The result of identifying 9th Kumano sample using MSdatanet.

6 Discussion

6.1 Application of CNN in Drone Captured Multispectral Images

In section 5.2, it was demonstrated that CNN-based analysis of MS images can effectively identify magnetite. In this paper, we aimed to verify the usefulness of a MS camera-equipped drone and tested the mineral identification capability by feeding the aerial images captured over the 9th Kumano area on the Kunisaki Peninsula to MSdatanet. As shown in Fig. 15, most of the areas were classified as white sands or hornblende, with some spots identified as magnetite. While the mineral distribution in the 9th Kumano area is not clear, it is unlikely that there are significant errors in the classification results, considering the XRD analysis results in section 4.1 showing that most minerals are white sands or hornblende. However, it should be noted that the experiments in section 5.2 were conducted in an ideal indoor environment, and there may be differences in data processing and imaging methods compared to outdoor drone imaging, where the pixel resolution may also differ.

Moreover, since we used a pre-existing drone with an MS camera for the experiments, the bands used in imaging could not be selected. For instance, Fig. 16 compares the waveform when augite is correctly identified as augite and when it is mistakenly classified as hematite. While the overall shape of the waveform is similar, there are differences in the spectral absorption levels around bands 2-3, which likely contributed to the different classification results.

Therefore, by identifying and selecting the bands that strongly affect mineral identification, it may be possible to develop an MS camera-equipped drone specialized in identifying specific minerals. In future studies, it is necessary to investigate the bands that strongly affect the identification of magnetite and ilmenite and explore how to deal with differences in sunlight conditions and resolutions.

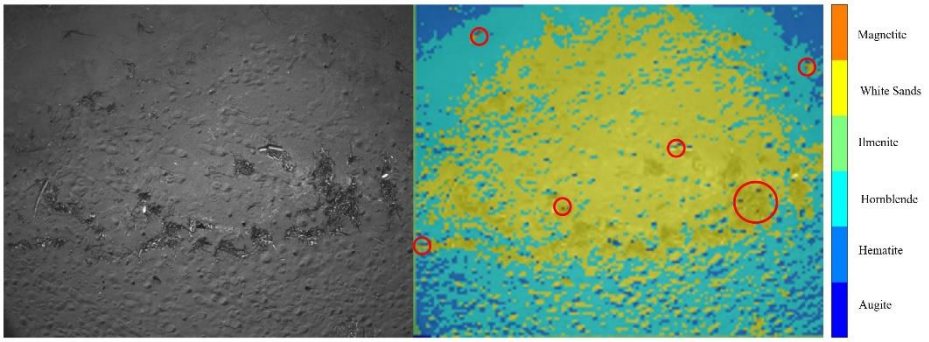

Fig. 15. Mineral classification results of the aerial photo using the MSdatanet model.

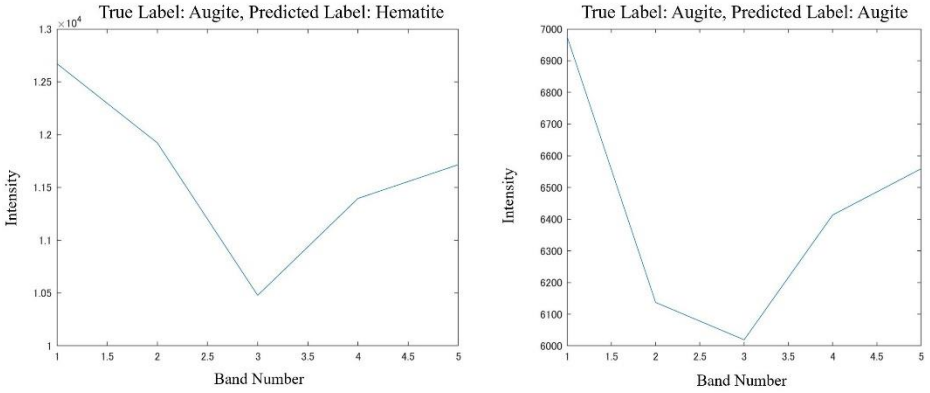

Fig. 16. Comparison of the waveforms when the MSdatanet model correctly identified augite as augite, and when it misclassified augite as hematite.

7 Conclusions

This study aims to evaluate an efficient approach for the automatic identification of mineral sand composition, using a commercial drone equipped with a MS camera and to verify the effectiveness of this approach in identifying mineral compositions in placer deposits. This verification is essential for developing a system using a MS technique for drone-based exploration of large-scale spaces, such as mineral sand deposits, and identifying target minerals and other valuable minerals using aerial exploration by drones.

The MS camera captures images of mineral deposits, which are analyzed using CNN to identify various minerals. Pre-processing of the data is conducted prior to training the AI algorithms. The process involves image segmentation, labeling each pixel in a captured image. XRD analysis was conducted on the beach sand collected from the field, revealing the presence of quartz, magnetite, and ilmenite. Rock specimens

containing various minerals were prepared and photographed using an MS camera in a darkroom, with the target minerals illuminated from three directions using halogen lights. The lighting position was adjusted to prevent shadows from occurring on the minerals, and photographs were taken from 40 cm above the target. In addition, a drone equipped with an MS camera captured images of the coastline of the Kunisaki peninsula.

Next, feature point matching corrected parallax errors among five TIF images, which were then stacked to create a data cube with information on five bands. Mineral data was selected from the cube, and wavelengths were extracted for each pixel as CSV files. A 2D CNN with 21 layers was utilized to classify the minerals. This brain, MSdatanet, was trained on 60,000 data sets of six mineral types and achieved a validation accuracy of 79.65%. While the model struggled to identify colored minerals, it was able to identify magnetite with 90% accuracy. When tested on sand samples from 9th Kumano, MSdatanet identified that the sample collected consisted largely of magnetite, hornblende, and Augite. Overall, MSdatanet seems a promising model for identifying magnetite in sand samples using MS imaging.

Finally, verification was made to test its mineral identification capability by feeding the aerial images captured over the 9th Kumano area to the MSdatanet model. The results showed that most of the areas were classified as white sands or hornblende, with some spots identified as magnetite. However, the experiments were conducted in an ideal indoor environment, and there may be differences in data processing and imaging methods compared to outdoor drone imaging, where the pixel resolution may also differ. It will be necessary to develop an MS camera-equipped drone specialized in identifying specific minerals by identifying and selecting the bands that strongly affect mineral identification. Future studies need to investigate the bands that strongly affect the identification of magnetite and ilmenite and explore how to deal with differences in sunlight conditions and resolutions.

Acknowledgement

The site of this research is owned by Yusei Tanaka. This research would not have been a success without the supervision, mentorship and support of professor Youhei Kawamura and Yoko Otomo. I would like to thank Natsuo Okada for the technical assistance and the study was improved by discussion with Brian Bino Sinaice. I am grateful to all my colleagues in the laboratory, scholarship organization and leading program for their comments, insights, and encouragement.

References

1. Rauhala, A.; Tuomela, A.; Davids, C.; Rossi, P. UAV Remote Sensing Surveillance of a Mine Tailings Impoundment in Sub-Arctic Conditions. *Remote Sensing* 2017, *9* (12), 1318. https://doi.org/10.3390/rs9121318.
2. Martelet, G.; Gloaguen, E.; Døssing, A.; Lima Simoes da Silva, E.; Linde, J.; Rasmussen, T. M. Airborne/UAV Multisensor Surveys Enhance the Geological Mapping and 3D Model

of a Pseudo-Skarn Deposit in Ploumanac'h, French Brittany. *Minerals* 2021, 11 (11), 1259. https://doi.org/10.3390/min11111259.

3. Sinaice, B. B.; Kawamura, Y.; Kim, J.; Okada, N.; Kitahara, I.; Jang, H. Application of Deep Learning Approaches in Igneous Rock Hyperspectral Imaging. In *Proceedings of the 28th International Symposium on Mine Planning and Equipment Selection - MPES 2019*; Topal, E., Ed.; Springer Series in Geomechanics and Geoengineering; Springer International Publishing: Cham, 2020, pp 228–235. https://doi.org/10.1007/978-3-030-33954-8_29.
4. Saha, D.; Annamalai, M. Machine Learning Techniques for Analysis of Hyperspectral Images to Determine Quality of Food Products: A Review. *Current Research in Food Science* 2021, S2665927121000034. https://doi.org/10.1016/j.crfs.2021.01.002.
5. Fox, N.; Parbhakar-Fox, A.; Moltzen, J.; Feig, S.; Goemann, K.; Huntington, J. Applications of Hyperspectral Mineralogy for Geoenvironmental Characterisation. *Minerals Engineering* 2017, 107, pp 63–77. https://doi.org/10.1016/j.mineng.2016.11.008.
6. Zhang, X.; Li, P. Lithological Mapping from Hyperspectral Data by Improved Use of Spectral Angle Mapper. *International Journal of Applied Earth Observation and Geoinformation* 2014, 31, pp 95–109. https://doi.org/10.1016/j.jag.2014.03.007.
7. Ganesh, U. K.; Kannan, S. T. Creation of Hyper Spectral Library and Lithological Discrimination of Granite Rocks Using SVCHR -1024: Lab Based Approach. *Journal of Hyperspect*
8. Weyermann, J.; Schläpfer, D.; Hueni, A.; Kneubühler, M.; Schaepman, M. Spectral Angle Mapper (SAM) for Anisotropy Class Indexing in Imaging Spectrometry Data. *Proceedings of SPIE - The International Society for Optical Engineering* 7457, 74570B-12. https://doi.org/10.1117/12.825991.
9. Hu, H.; Feng, D.-Z.; Chen, Q.-Y. A Novel Dimensionality Reduction Method: Similarity Order Preserving Discriminant Analysis. *Signal Processing* 2021, 182, 107933. https://doi.org/10.1016/j.sigpro.2020.107933.
10. So, H.; Satoshi, T. Estimation of Chlorophyll content in leaves of *Abies sachalinensis* using NDVI imagery. 133rd Annual JFS Meeting, 133, 2022. https://doi.org/10.11519/jfsc.133.0_310,
11. Akira, H.; Kei, T.; Bin, C.; Akihiko, K.; Examination of appropriate observation time and correction of vegetation index for drone-based crop monitoring. *Journal of Agricultural Meteorology* 2021, 77 (3), pp200-209. https://doi.org/10.2480/agrmet.D-20-00047,
12. Dominic, F.; Cinzia, P.; Giulia, T.; Mirco, B.; Marco, C,; Anton, E,; Khelvi, B.; Roberto, C.; Franco, M.; Uwe, R.; Karen, A.; Multi-Scale Evaluation of Drone-Based Multispectral Surface Reflectance and Vegetation Indices in Operational Conditions *Remote Sensing* 2020, *12*(3), 514. https://doi.org/10.3390/rs12030514
13. Masashi, K.; Fumio, K.; Shuji, M. 未利用鉄資源開発調査について. 鉱山地質, 8 (30), 1958, pp 243-255. https://doi.org/10.11456/shigenchishitsu1951.8.30_243
14. Ziro, N.; Syuji, M.; On the Titaniferous Iron Sand Ore Deposits at the Kunisaki Peninsula, Ooita Prefecture. 地質調査所月報 8 (5), 1957.
15. Sharma, N.; Sharma, R.; Jindal, N. Machine Learning and Deep Learning Applications-A Vision. *Global Transitions Proceedings* 2021, S2666285X21000042. https://doi.org/10.1016/j.gltp.2021.01.004.
16. Fox, N.; Parbhakar-Fox, A.; Moltzen, J.; Feig, S.; Goemann, K.; Huntington, J. Applications of Hyperspectral Mineralogy for Geoenvironmental Characterisation. *Minerals Engineering* 2017, 107, pp 63–77. https://doi.org/10.1016/j.mineng.2016.11.008.
17. van der Meer, F. D.; van der Werff, H. M. A.; van Ruitenbeek, F. J. A.; Hecker, C. A.; Bakker, W. H.; Noomen, M. F.; van der Meijde, M.; Carranza, E. J. M.; Smeth, J. B. de; Woldai, T. Multi- and Hyperspectral Geologic Remote Sensing: A Review. *International*

Journal of Applied Earth Observation and Geoinformation 2012, 14 (1), pp 112–128. https://doi.org/10.1016/j.jag.2011.08.002.

18. Heinz-H. Erbe, John E., Udd ,J. Sasiadek (2004). *Mining Automation. IFAC Proceedings*, Volume 37(5), 2004, pp 299-304. https://doi.org/10.1016/S1474-6670(17)32384-4
19. Beretta, F.; Rodrigues, A. L.; Peroni, R. L.; Costa, J. F. C. L. Automated Lithological Classification Using UAV and Machine Learning on an Open Cast Mine. *Applied Earth Science* 2019, 128 (3), pp 79–88. https://doi.org/10.1080/25726838.2019.1578031.
20. Mohajane, M.; Essahlaoui, A.; Oudija, F.; El Hafyani, M.; Cláudia Teodoro, A. Mapping Forest Species in the Central Middle Atlas of Morocco (Azrou Forest) through Remote Sensing Techniques. *IJGI* 2017, 6 (9), 275. https://doi.org/10.3390/ijgi6090275.
21. Yasushi, Y.; Ippei, T.; Mineralogical mapping by ASTER in Cuprite, Nevada, U.S.A. *Asian J. of Geoinf.*, 3 (3), pp 17-24, 2003.
22. Yasushi, Y.; C. Naito,; Spectral indices for lithologic discrimination and mapping by using the ASTER SWIR bands, *Int. J. of Remote Sensing* 24 (22), pp 4311-4323, 2003.
23. Jitendra, S. K.; Atul, K.; Subhash, P.; Rishi, S. Amol, G.; Shyam, G,; Comparative Study of Regressor and Classifier with Decision Tree Using Modern Tools. *Materials Today. Proceedings*, 56(6), 2021. pp 3571-3576. https://doi.org/10.1016/j.matpr.2021.11.635
24. Ahmad, A., A, S.; Mohsen, A., R.; Self Learning Machines Using Deep Networks. In 2011 International Conference of Soft Computing and Pattern Recognition (SoCPaR); *IEEE*: Dalian, China, 2011, pp 21–26. https://doi.org/10.1109/SoCPaR.2011.6089108
25. Anand, V.; Markus, G.; Norman, K,; Francesco, N.; Disaster damage detection through synergistic use of deep learning and 3D point cloud features derived from very high resolution oblique aerial images, and multiple-kernel-learning. *ISPRS Journal of Photogrammetry and Remote Sensing*. 140, 2018, pp45-49.DOI: 10.1016/j.isprsjprs.2017.03.001
26. Mohammadi, M.; Rezaei, J.; Ensemble Ranking: Aggregation of Rankings Produced by Different Multi-Criteria Decision-Making Methods. *Omega*, 96, 2020, 102254.

Open Access This chapter is licensed under the terms of the Creative Commons Attribution-NonCommercial 4.0 International License (http://creativecommons.org/licenses/by-nc/4.0/), which permits any noncommercial use, sharing, adaptation, distribution and reproduction in any medium or format, as long as you give appropriate credit to the original author(s) and the source, provide a link to the Creative Commons license and indicate if changes were made.

The images or other third party material in this chapter are included in the chapter's Creative Commons license, unless indicated otherwise in a credit line to the material. If material is not included in the chapter's Creative Commons license and your intended use is not permitted by statutory regulation or exceeds the permitted use, you will need to obtain permission directly from the copyright holder.